IEEE Open Journal of
Antennas and Propagation

Received 5 December 2022; revised 31 December 2022; accepted 17 January 2023. Date of publication 23 January 2023; date of current version 7 February 2023.

Digital Object Identifier 10.1109/OJAP.2023.3238706

A Deployable Wideband Differential-Fed Dual-Polarized Patch Antenna Array

ANKANG LIU (Member, IEEE), JIAN LU (Senior Member, IEEE), PENG KHIANG TAN, AND THENG HUAT GAN (Member, IEEE)

National University of Singapore, Singapore 119077

CORRESPONDING AUTHOR: T. H. Gan (e-mail: thenghuat@nus.edu.sg).

ABSTRACT In this paper, a deployable wideband differential-fed dual-polarized high-isolation patch antenna array is proposed. To achieve dual polarization, every element has two pairs of differential ports. Because of the differential design, the couplings from the adjacent ports (the other pair of ports) are canceled and high isolation between the two polarization is achieved. In addition, capacitive feeds are applied to enhance the bandwidth. By integrating with two planar Marchand baluns, the two pairs of the differential ports are excited for dual polarization. Then, the wideband dual-polarization patch antenna element is expanded to a 4×4 antenna array for better gain. In order to achieve deployment, we present a novel foldable mechanism suitable for low-frequency patch antenna array, which is different from the conventional design on the flexible printed board. The deployment concept is presented. One prototype is fabricated and measured. Its operating band is from 1.15 GHz to 1.35 GHz. The peak gains of the two polarizations are 14.4 dBi and 14.1 dBi respectively.

INDEX TERMS Deployable antenna, dual-linear polarization, high isolation, wideband patch antenna array, Marchand balun.

I. INTRODUCTION

IN RECENT years, interest in deployable antennas has been growing exponentially. The deployable dual-polarization patch antenna array is a potential candidate due to its small size, light weight, high gain, and ability to duplicate the band [1].

Due to the flexibility and low mass density of flexible printed circuit boards (FPCB), they are widely used to deploy patch antennas. Different patterns such as the patch, the ground layer and the stacked patch, are printed on different layers of FPCB. In [2], Huang proposes an impressive paper-thin membrane aperture-coupled L-Band Antennas. Based on the antenna presented in [2], an active membrane phased array is developed [3]. Membrane compatible Transmit/Receive (T/R) modules are applied for each antenna element. However, this paper does not introduce the deployment method for maintaining the distance between different layers. Hashemi et al. presents an insightful flexible X-band phased array system with low areal mass density in [4]. A collapsible feeding transition is used. However, such deployment design is suitable for high frequency applications where the physical height is considered relatively low. It could be challenging to apply this deploy mechanism for the low-frequency applications.

Various dual-polarized high-isolation patch antennas have been proposed and studied [5], [6], [7], [8], [9], [10], [11], [12], [13], [14], [15], [16]. According to the feeding mechanism, the dual-polarized patch antenna are classified into three categories: (1) dual-slot-fed patch antenna, (2) hybrid-fed patch antenna, and (3) differential-fed patch antenna.

The dual-slot-fed dual-polarized patch antenna uses two orthogonal slots to excite two linear polarizations. The dual-slot-fed patch antenna is proposed in 2004 by Ghorbani and Waterhouse [5]. In addition to the resonances of the patch and the coupling aperture, a stack patch is also applied to generate the third resonance. As such, the antenna can achieve a bandwidth of over 50%. A reflector is added under the slots to increase the front-to-back ratio (FTBR). Then based on [5], many variant designs are developed. In [6], [7], two deployable series-fed dual-polarized flexible antenna arrays are presented. In [8], a 7-layer patch antenna achieves over 95% bandwidth by means of the modified slots. In summary, the dual-slot-fed antennas requires at least 4 layers including

a patch, a ground plane, a slot layer and a reflector (for high FTBR).

The hybrid-fed patch antenna has two different feeding mechanisms. This hybrid feed can be the combination of the slot feed, the direct feed, the differential feed or the L-probe feed. Wong and Chiou develop several hybrid-fed antennas [9], [10], [11]. These designs all have an aperture-coupled feed while the other is a pair of differential probe feeds or a L-probe feed. Then in [12], [13], [14], slot feed and differential feed are applied to excite two polarizations. In [14], a novel millimeter-wave dual-polarized 2-dimensional (2D) multibeam antenna array with the slot and the differential feed is presented. By using the substrate integrated waveguide (SIW) technology to realize the array, the structure becomes complex and bulk. Although compared with the dual-slot-fed patch antenna, the hybrid feed patch antenna require less layers, it is still not considered as a good choice for a the deployable antenna array due to the complicated layout and large size.

For the differential-fed patch antenna, as its name suggests, the dual polarization of the antenna is excited by two pairs of differential feeds. In [15], a 180° broadband balun enables the antenna to have 50% bandwidth, but at the expense of the antenna size. Due to well-designed ring hybrid coupler, a differential-fed patch antenna achieves an impressive 90 dB isolation between its two ports [16]. However, coaxial cables and independent loop hybrid coupler reduces the compactness of the antenna. Although the layer number of the differential-fed patch antenna is further reduced, the sizes of the previous designs are considered to be too large for the deployable antenna array.

Considering the complexity and large size of previous differential dual-polarized patch antennas, a simple and compact wideband design is proposed. Unlike the large baluns applied on previous designs [15], [16], two compact Marchand baluns are placed under the patch to excite two pairs of differential ports while maintaining the antenna size smaller than $\lambda/2 \times \lambda/2$. The preliminary concept is introduced in our conference paper [17]. The antenna is successfully expanded to a 4×4 array via a cooperate feeding network. The array antenna is designed as a receiver. The frequency band of interest is from 1.15 GHz to 1.35 GHz with a return loss of 6 dB. A novel mechanism is also developed for the deployment of the proposed low-band antenna arrays. In Section II, the design and principle of the antenna element are introduced. Then the antenna array development is presented in Section III. In Section IV, the details of the deployment mechanism are documented. The measurement and simulation results are also shown and compared in this section.

II. DUAL POLARIZATION PATCH ANTENNA ELEMENT

In this section, the antenna element is introduced first, then followed by the wideband planar Marchand balun. The antenna element integrated with the balun is also studied. All the simulations are conducted using ANSYS HFSS.

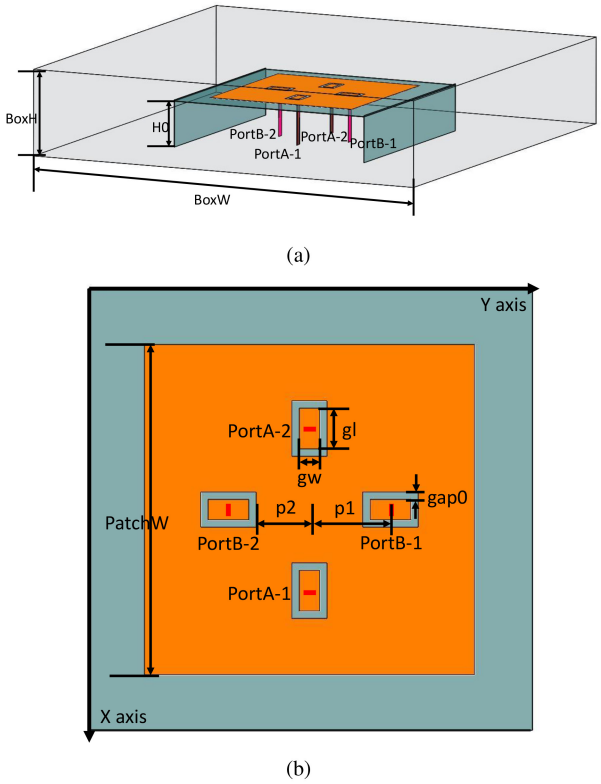

FIGURE 1. Structure of the dual-polarized antenna element. (a) 3D view. (b) Top view.

A. ANTENNA ELEMENT

The differential-fed patch element is shown in Fig. 1. Its patch is designed on the low-cost FR4 substrate (grey part as shown in Fig. 1) with a dielectric constant of 4.4 and a loss tangent of 0.02. In order to reduce the antenna weight, the thickness of the substrate is selected to be 0.508mm. The dielectric between the ground and the patch is air, whose thickness is 20 mm. In the simulation model, the four sides of the airbox are set as the master-slave boundary. The top and the bottom surfaces are set as the radiation and Perfect Electric Conductor (PEC) boundaries respectively.

The four ports are divided into two differential pairs (Port A-1 pairs with Port A-2 and Port B-1 pairs with Port B-2). The two ports of each pair are out of phase and equally excited. In this way, each differential pair is used to excite one linear polarization. The isolation between the two polarization also benefits from the differential-fed design. In conventional design methods, in order to achieve high isolation, the coupling between different polarization should be as low as possible by optimizing the feed position. In the proposed feed mechanism, the locations of the feeds are not critical parameter to obtain high isolation. The high isolation is naturally obtained via the differential feed mechanism. For example, as shown in Fig. 2(b) and 2(c), although the coupling from Port B-1 and Port B-2 to Port A-1 is strong, they are equal and out of phase and thereby, can cancel each other. As such, a high degree of isolation is achieved.This

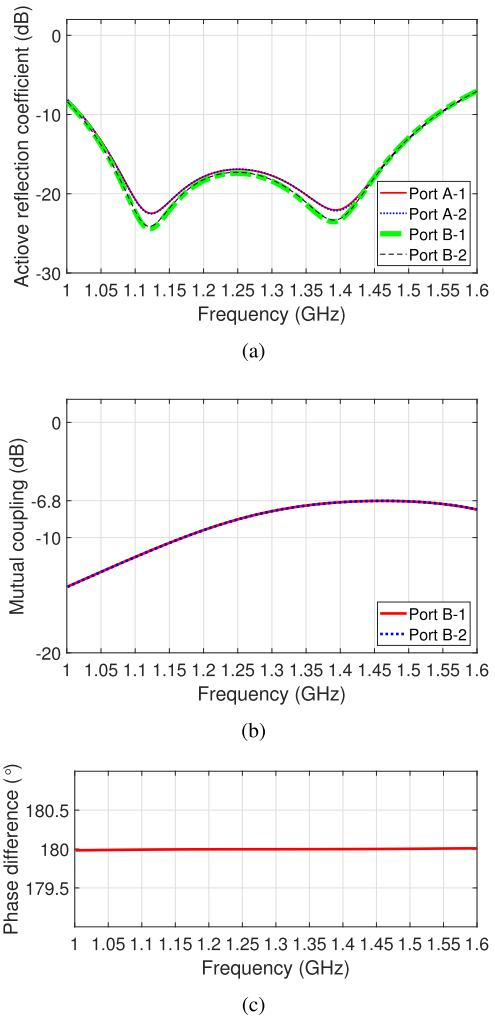

FIGURE 2. (a) Simulated reflection coefficients of the dual-polarized antenna element. (b) Simulated coupling amplitudes from Port A-1 to Port B-1 and Port B-2. (c) Simulated phase difference of the coupling from Port A-1 to Port B-1 and Port B-2.

also applied to the coupling between Port B-1 and Port B-2 to Port A-2.

One should notice that there are gaps between the feeds and the patch (Fig. 1(b)). These gaps are considered as proximity feeds. As the capacitance of the gap and the inductance of the probe formed a LC resonator, an additional resonance is generated. This resonance enhances the frequency bandwidth of the patch antenna. By comparing the active reflection coefficients between the patch designs (Fig. 2(a) and Fig. 3), it can be found that the design with the etched gap has dual resonances, which significantly increases the bandwidth of the patch antenna. The radiation patterns for both polarizations of the proposed patch antenna are shown in Fig. 4. These radiation patterns are similar with peak gains of 6.2 dBi.

B. MARCHAND BALUN

In order to obtain a wide band differential signal, a planar Marchand balun is required, which exhibits simple and compact structure with stable performance over a wide bandwidth [18], [19], [20], [21]. The proposed planar Marchand

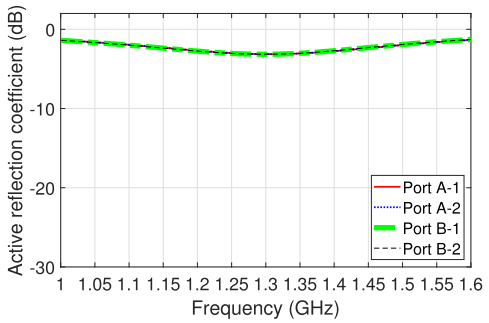

FIGURE 3. Simulated reflection coefficients of the dual-polarized antenna element without gaps.

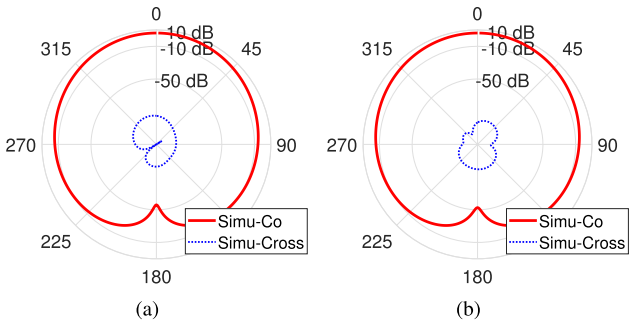

FIGURE 4. Simulated radiation patterns in H plane. (a) Port A-1 and Port A-2 are excited at 1.5 GHz. (b) Port B-1 and Port B-2 are excited at 1.5 GHz.

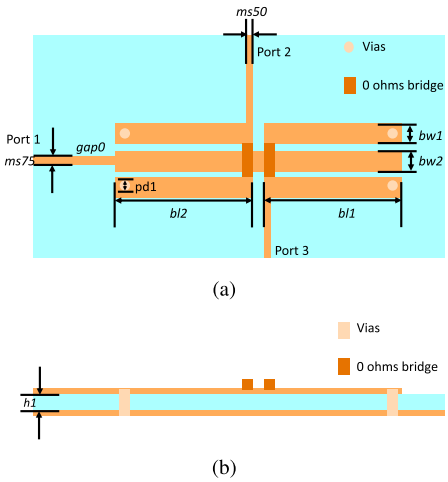

FIGURE 5. Structure of the Marchand balun. (a) Top view. (b) Cross section view.

balun is shown in Fig. 5. Unlike those previous planar wideband Marchand balun designed in [19], [20], the proposed balun is constructed with full ground without any slot. As such, the balun can be placed on any surface without affecting its performance.

The balun is applied to transfer the single-ended signal at Port 1 to a pair of differential signals at Port 2 and Port 3, which are equal in magnitude but out of phase. In the proposed design, the impedance of Port 1 is 75 Ω while the impedance of Port 2 and Port 3 is set as 50 Ω. The substrate used for the Marchand balun is Rogers 4003, with a dielectric constant of 3.55 and

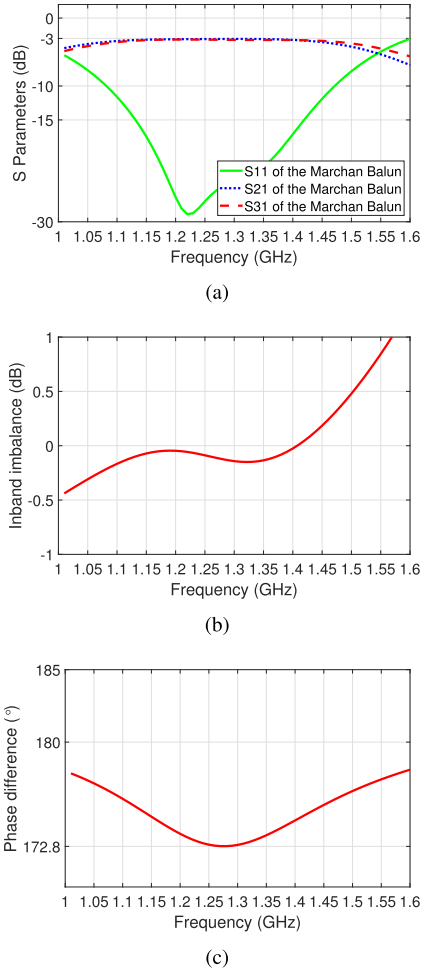

FIGURE 6. (a) Simulated S parameters of the Marchand Balun. (b) Simulated imbalance between Port 2 and Port 3. (c) Simulated phase difference between the output at Port 2 and Port 3.

a loss tangent of 0.0027. Its parameters are as follows: $ms75$=0.55 mm, $ms50$=1.15 mm, $bw1$=3 mm, $bw2$=1.4 mm, $gap0$=0.2 mm, $bl1$=$bl2$=36 mm, $pd1$=1 mm, and $h1$=0.508 mm.

The simulated scattering parameters (S parameters) are shown in Fig. 6. The −10 dB bandwidth of the balun is 36.5%. The simulated in-band imbalance varies from −0.22 dB to 0.29 dB and the phase difference between Port 2 and Port 3 is from −172.8° to −177.8°.

C. ANTENNA ELEMENT INTEGRATED WITH MARCHAND BALUN

The antenna element (in Section II-A) fed by two Marchand baluns (in Section II-B) is shown in Fig. 7(a). It consists of two PCBs. The substrate of the top PCB is FR4, where the patches are printed on it. The bottom one uses Rogers 4003 as the substrate and printed with planar baluns. The distance between the two boards is 19.492 mm ($H0-h1$). The patch antenna and the balun shares one ground plane. Through rotating one of the baluns, as demonstrated in Fig. 7(b), the two Marchand baluns are judiciously placed under the

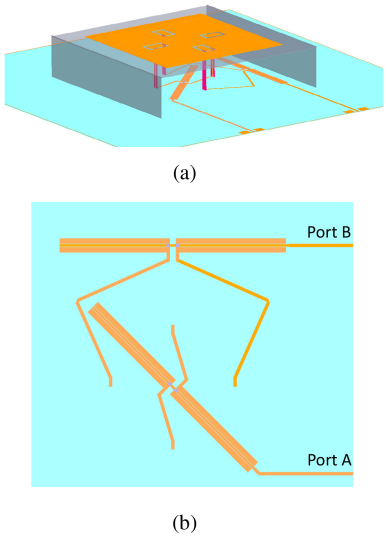

FIGURE 7. (a) Antenna element integrated with the Marchand balun. (b) Layout of the two Marchand baluns on the bottom layer.

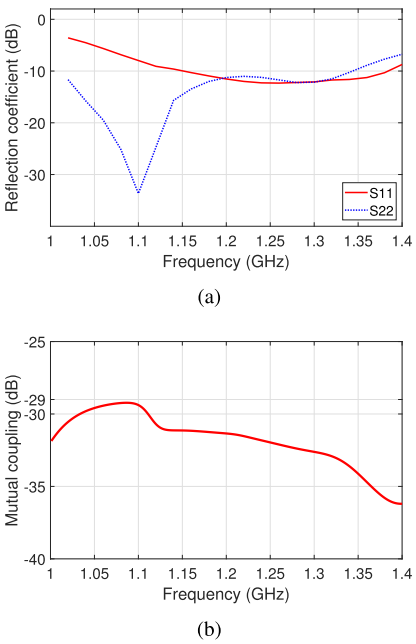

FIGURE 8. (a) Simulated reflection coefficients of the integrated antenna element (S11 corresponds to Port A while S22 corresponds to Port B). (b) Simulated mutual coupling between Port A and Port B.

patch antenna. The balanced ports of these Marchand baluns are separately connected to the two differential feeds of the patch antenna. With such an arrangement, dual polarization is excited. In the full wave simulation, the boundary settings for the integrated antenna is the same as those of the antenna element described in Section II-A.

The simulation results of the integrated antenna element are shown in Fig. 8. The −10 dB bands for Port A and Port B are from 1.13 GHz to 1.39 GHz (20.6%) and from 1.01 GHz to 1.35 GHz (28.8%) receptively. The bands of both the two ports can cover the desired band (1.15 GHz

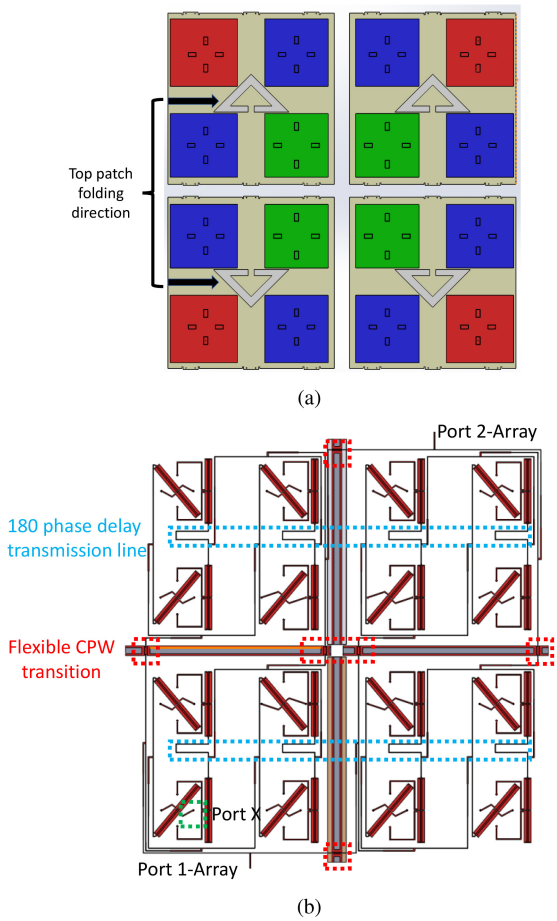

FIGURE 9. (a) Pattern of the top PCB (top patch board). (b) Feeding network pattern of the bottom PCB (bottom board).The split triangular show the folding direction of the patch.

to 1.35 GHz). In addition, the isolation between Port A and Port B is higher than 29 dB.

III. ANTENNA ARRAY

Considering the gain of the patch antenna is not as high as others kinds of antennas [22], the integrated element is expanded to a 4×4 antenna array as shown Fig. 9. Similarly, it also consists of two two-layer-PCBs. The top PCB (Fig. 9(a)) is printed with the antenna pattern while the bottom PCB is for the feeding network (as shown in Fig.9(b)) and the shared ground respectively. Considering the foldability of the antenna array, both PCBs are divided into four parts. Each part consists of an 2×2 sub-array. The top four parts are isolated from each other while the four bottom boards are interconnected with flexible printed circuit broads (FPCBs). The details of the mechanical design are discussed and demonstrated in Section IV.

As shown in Fig. 9(a), according to the location, the elements in the array are labeled as "Internal", "Edge" and "Corner" elements, which are marked as green, blue and red respectively. Generally, even all the elements are identical, the active matching properties of these three types of element

TABLE 1. Boundary settings for "edge" and "corner" simulation models.

Excitation	Top	Bottom	B1	B2	B3	B4
Port A1 and Port A2 ("Edge")	Rad	Rad	PEC	PMC	PEC	Rad
Port B1 and Port B2 ("Edge")	Rad	Rad	PMC	PEC	PMC	Rad
Port A1 and Port A2 ("Corner")	Rad	Rad	PEC	PMC	Rad	Rad
Port B1 and Port B2 ("Corner")	Rad	Rad	PMC	PEC	Rad	Rad

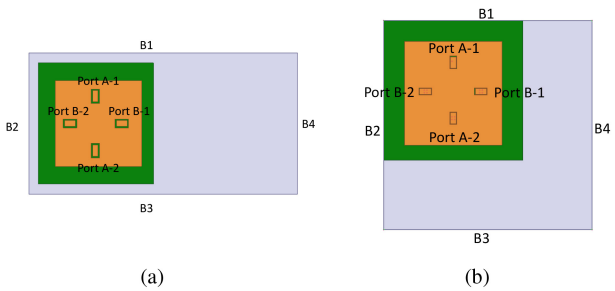

FIGURE 10. Top view of optimizing model. (a) Edge element. (b) Corner element.

are not similar due to the edge effect, where the performance of the "Edge" and"Corner" elements may be poorer than that of the "Internal" element. Typically, this does not affect the performance of a large-scale antenna array. However, for a relatively small array (e.g., a 4 × 4 array), this effect cannot be neglected. In this case, besides optimizing the "Internal" element using the master-slave boundary with one single element model, different simulation models are needed for optimizing the active matching properties of the "Edge" and "Corner" elements.

The top view of the simulation model for the "Edge" and "Corner" elements is shown in Fig. 10. Due to proximity effect, the boundary settings for different polarization optimizations have to be different. The boundary settings for different polarization and different element types are listed in Table 1.

The comparison between the reflection coefficients of the elements before and after optimization is shown in Fig. 11. The unoptimized results are referred to the reflection coefficients obtained by simulating the integrated elements developed in Section II-C with the boundary settings listed in Table 1. It can be found that the reflection coefficients of the "Edge" and "Corner" elements are significantly improved after optimization at the interested band (1.15 GHz to 1.35 GHz).

The feeding network is shown in Fig. 9(b). Two 16-way power dividers are used to feed the baluns. The inputs of the two power dividers are labeled as "Port 1-Array" and "Port 2-Array". Each power divider corresponds to one polarization. Due to the size of the antenna array, the feeding network is already very crowded. Even worse, spare space needs to be left for the deployment mechanical devices. Therefore,

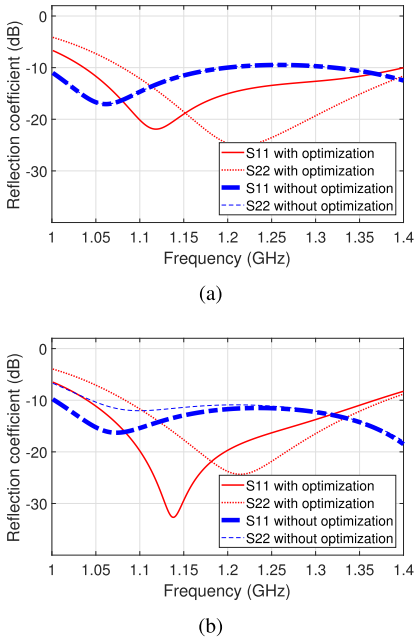

FIGURE 11. S11 and S22 with/without optimization (S11 corresponds to Port A-1 while S22 corresponds to Port A-2). (a) Edge element. (b) Corner element.

the feeding network needs to be simplified. First, the second and fourth rows of the Marchand balun are flipped vertically. Then 180° phase delay transmission line at the center frequency (circled in blue shown in Fig. 9(b)) are needed to compensate the phase difference caused by the flip

As mentioned in the first paragraph of this section, in order to achieve the foldability of the antenna array, FPCBs are used to bridge between the adjacent ridge feeding network boards. Since the substrate of the FPCB is relatively thin, the transmission line should be constructed as a co-planar waveguide (CPW) rather than a microstrip line (ML). Therefore, a ML-CPW-ML transition is designed as shown in Fig. 12(a) and 12(b). The values of the characteristic impedance of the ML and the CPW are the same. Vias are used to connect the ML and the center strip of the CPW. The ground of the ML and the CPW are connected. The simulation results of a ML-CPW-ML transition can be found in Fig. 12(c). From 1 GHz to 1.6 GHz, the reflection loss is better than 20 dB and the insertion loss is less than 0.1 dB.

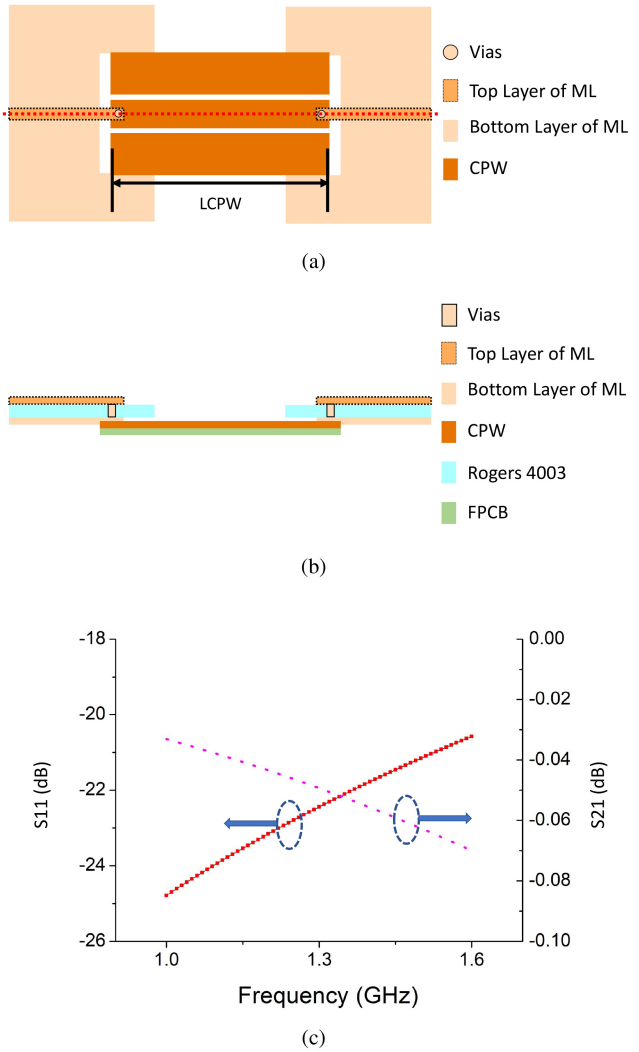

FIGURE 12. (a) Top view of the ML-CPW-ML transition without the PCB (Metal only). (b) Cross section view of the ML-CPW-ML transition. (c) Simulated S parameters of the transition.

IV. ANTENNA DEPLOYMENT AND PERFORMANCE

In order to verify the design strategy, a prototype of the proposed wideband dual-polarized antenna array is fabricated and tested.

The components of the deployable antenna array is shown in Fig. 13. The patterns of the top patch in one array are identical but with different orientation. The side PCBs perform as the support for the top PCB and define the distance between the top and bottoms boards. The probe is flexible and made of FPCB. In addition, it is worth mentioning that customized hinges were developed to connect the side PCB and top/bottom PCB. The three-dimensional

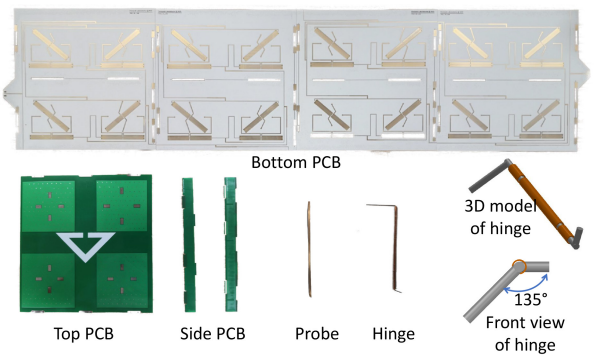

FIGURE 13. Components of the antenna array.

(3D) Solidworks model is also shown for more details. Due to the height requirement in the stored state, the hinge used for the collapsible antenna must be small. The diameter of the hinge is expected to be no more than 2mm. As far as

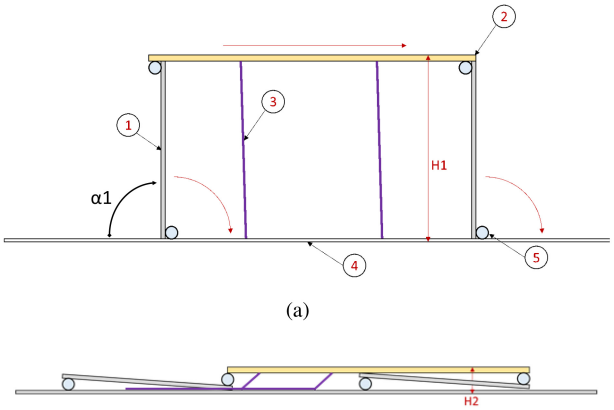

FIGURE 14. Schematic diagram of the folding process of the top patch. (a) Deployed. (b) Folded. (① to ⑤ refer to side PCB, normal hinge, probe, bottom PCB and self-closing hinge.)

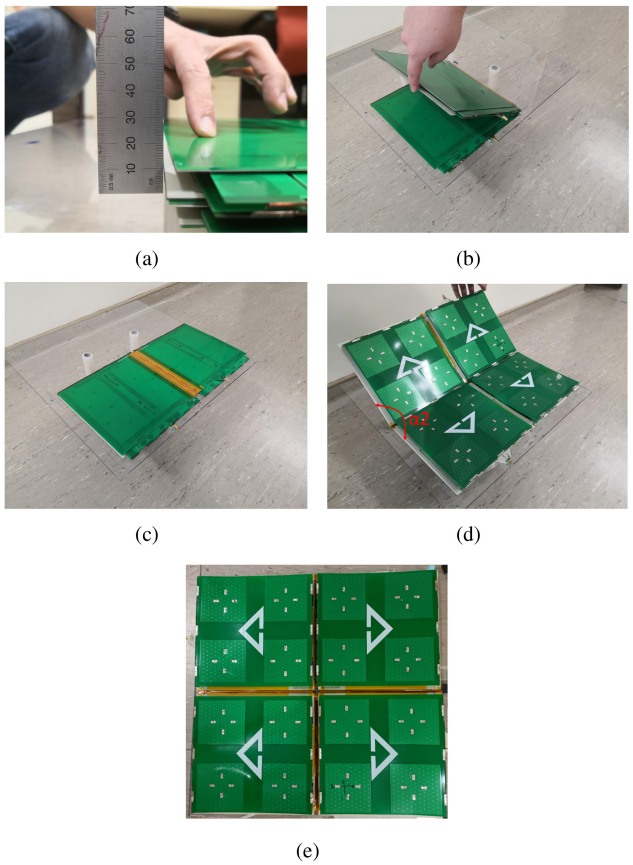

FIGURE 15. Deployment process of the antenna array. (a) Step 1. (b) Step 2. (c) Step 3. (d) Step 4. (e) Fully deployed array.

the authors know, there is no commercial hinge that can meet this requirement. So, we designed and manufactured the hinge by ourselves. The tube (brown) is made of the semi rigid coaxial cable with the internal core removed. It is cut into three parts. The internal pin (silver) is made of the spring steel wires. There are two kinds of hinges: normal hinge and self-closing hinge. The normal hinges are applied to connect the side PCBs and the top PCBs, allowing the rotation between them. The two arms of the normal hinge are parallel to each other. The self-closing hinge is a modified version of normal hinge and is applied to force the top PCB deploy in addition to its rotation function. As such, the self-closing hinge has arms bent with an angle of 135°. The self-closing hinges are applied to connect the side PCBs and the bottom PCBs. When external force is added, the folding process of the top patch with the aid of the hinges is shown in Fig. 14. The deployment process is the reverse.

The prototype of the fully-deployed antenna array is shown in Fig 15(e). Its deployment has two procedures: bottom board deployment and top patch board deployment. Since the board-to-board connection is FPCB, the bottom board can be easily opened in the first-step deployment as shown in Fig. 15(a) to 15(d). During Step 4 as shown in Fig. 15(d), the external force on the patch board is withdrawn and the top patch pop upwards with the rotation of the customized self-closing hinges. The distance between the top and bottom boards is maintained by the rigid side PCB. The dimensions of the stored antenna array are 15mm×240mm×260mm while the dimensions of the deployed array are 20.5mm×480mm×520mm.

The deployment process degrades the reliability of the electrical connectivity for two components. The first is the flexible CPW transition and the second is the flexible probe. The flexible CPW transition's reliability for the electrical connectivity between the FPCB and rigid PCB is improved by soldering and then applying polyimide tape on the soldering joints. The improved flexible CPW transition is bent 10 times and electrical connectivity is not affected. The flexible probe has similar degradation for the electrical connectivity due to deployment process. After deployment, a few of the flexible probes become disconnected from the bottom boards. It is suspected that the soldering joints between the flexible probes and feeding network on the bottom board are weak. A possible solution is to increase the soldering area of the flexible probe and the connecting feeding network of the bottom board.

All the following measurement results are obtained after deployment. The simulated and measured S parameters are shown in Fig. 16. In the operating band (1.15 GHz to 1.35 GHz), the return losses of the two ports are both better than 6 dB while the coupling isolation between the Port 1-Array and Port 2-Array is over 30 dB.

The simulated and measured radiation patterns at 1.1 GHz and 1.35 GHz is shown in Fig. 17. The radiation patterns in E-plane and H-plane are obtained when the two ports are excited respectively. Their normalized cross-polarization is below −20 dB.

As shown in Fig. 18(a), the simulated peak realized gains of the two polarizations are 15.4 dBi and 15.3 dBi respectively while the measured peak gains are 14.4 dBi and 14.1 dBi. The difference between the simulated and measured gains is due to the loss of the feeding network (over 1 dB), the connectors loss (0.2 dB), the loss of probes

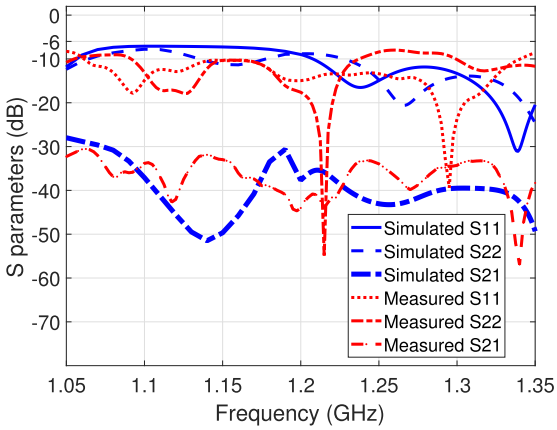

FIGURE 16. Simulated and measured S parameters (S11 corresponds to Port 1-Array while S22 corresponds to Port 2-Array).

(0.05 dB) and the loss of flexible transition (0.03 dB). (To speed up the simulation, the FPCB of the probes and the flexible transition were not included.) The simulated and measured insertion loss between Port 1-Array and Port X of the feeding network (as marked in Fig. 9) is shown in Fig. 19. When measuring the insertion loss, all the ports are terminated with 50 Ω resistors except the measured ports. It can be found that the measured loss of the feeding network is over 1 dB higher than the simulated one. In addition, the fabrication and the measurement errors could also lead to difference in gain between simulation and measurement.

The simulated and measured aperture efficiencies are shown in Fig. 18(b). In this article, the aperture efficiency of an array antenna, AE, is defined as:

$$AE = Gr/\left(4 * pi * A/\lambda_0^2\right) \tag{1}$$

where Gr is the realized gain, A is the area of the antenna aperture and λ_0 is the free-space wavelength. The measured efficiencies of the two ports is better than 47% and 50% respectively.

More tests have also been conducted to check the antenna performance with different deployment status. The first parameter is the angle between the side PCB and the ground, which is marked as $\alpha 1$ (refer to Fig. 14(a)). The ideal value should be 90°. The measured gain fluctuations of Port 1 versus the deviation of $\alpha 1$ at 1.25 GHz is shown in Fig. 20. It can be found that the gain fluctuation is always within $\pm$ 0.2 dB. Another parameter is the angle between the bottom PCB boards, which is marked as $\alpha 2$ (refer to Fig. 15(d)). The ideal value should be 180°. The measured gain fluctuations of Port 1 versus the deviation of $\alpha 2$ at 1.25 GHz is shown in Fig. 20. When the deviation is 10°, the gain drop is only 0.2 dB. While the 10° deviation is of low accuracy, which can be easily avoided in the real world. Overall, our design is not sensitive to the deployment status.

The comparison between the proposed antenna with the state-of-the-art deployable patch antennas is made in Table 2. It can be found that most of the deployable

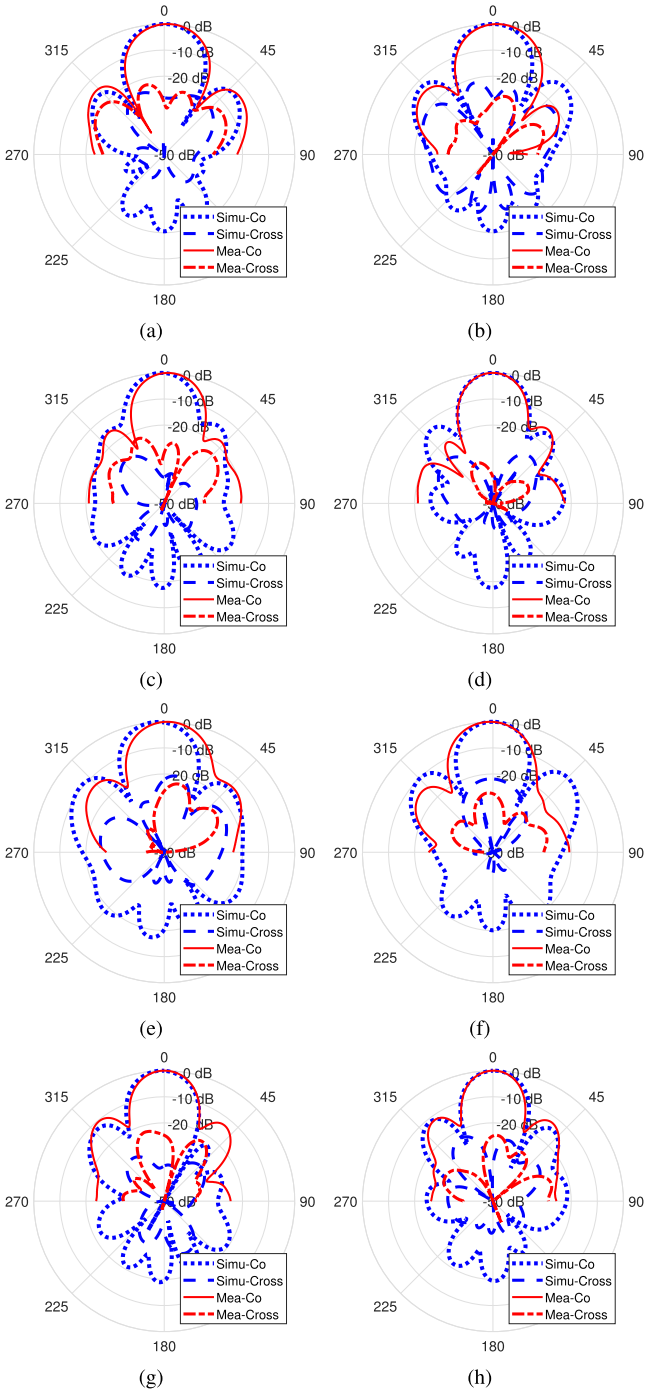

FIGURE 17. The radiation patterns of the antenna array. (a) E-plane at 1.15 GHz when Port 1-Array excited. (b) H-plane at 1.15 GHz when Port 1-Array excited. (c) E-plane at 1.35 GHz when Port 1-Array excited. (d) H-plane at 1.35 GHz when Port 1-Array excited. (e) E-plane at 1.15 GHz when Port 2-Array excited. (f) H-plane at 1.15 GHz when Port 2-Array excited. (g) E-plane at 1.35 GHz when Port 2-Array excited. (h) H-plane at 1.35 GHz when Port 2-Array excited.

patch antenna arrays are designed at higher frequency [4], [24], [25], [26], [27] due to the physical size of the patch antenna element. These working at L band or even lower have two limitations [3], [23]. The first one is the bandwidth. Foldable patch antenna arrays normally use thin substrates and cannot achieve wide bandwidth. The other is

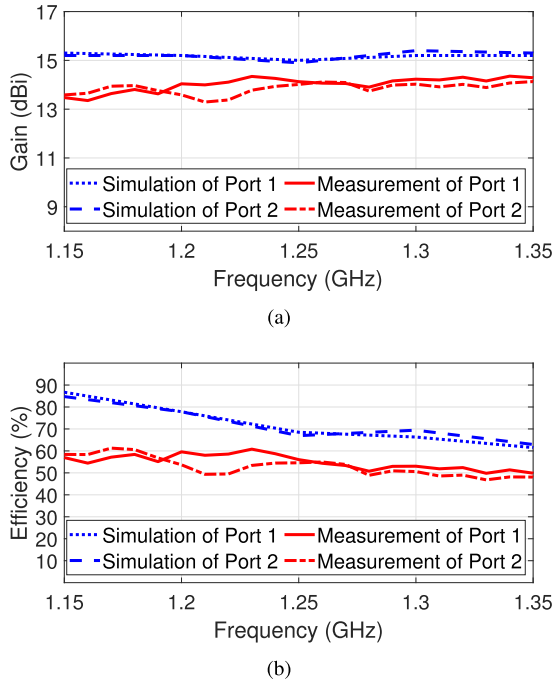

FIGURE 18. (a) Simulated and measured gains. (b) Simulated and measured aperture efficiencies.

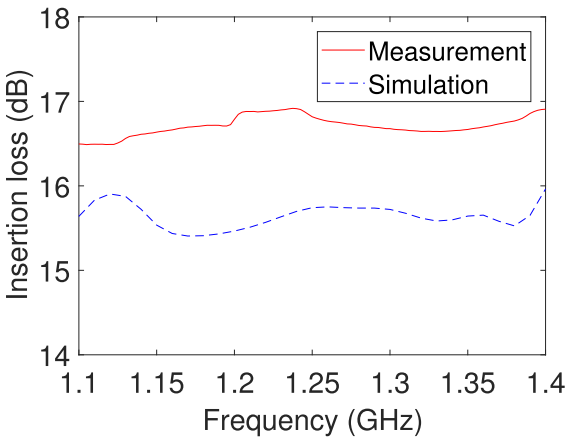

FIGURE 19. Simulated and measured insertion loss of the feeding network.

the array size. The previous deployment methods support antenna arrays with number of elements not larger than 8. Our proposed deployable array has 16 elements while maintains 16% fractional bandwidth. A volume reduction of 80% is achieved. In addition, our design achieves dual linear polarization and has the potential to realize circular polarization and polarization track if some other frontend devices are added. If the feeding network is further optimized like using multi-stage design and S11 of the array antenna can be improved to be better than −10 dB.

V. CONCLUSION

In this paper, a deployable wideband differential-fed dual-polarized high-isolation 4 × 4 patch antenna array is proposed. Every element has two pairs of differential probe feeds to excite two linear polarizations. The capacitive feed

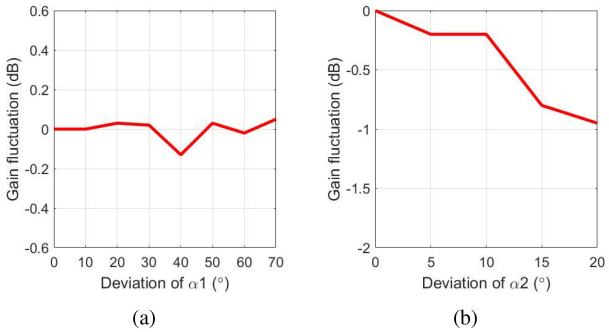

FIGURE 20. (a) Measured gain fluctuations of Port 1-Array versus (a) $\alpha 1$. (b) $\alpha 2$.

TABLE 2. Comparisons between the proposed antenna with the state-of-the-art deployable patch antennas.

Design	Realized gain (dB)	Bandwidth Criteria	Fractional Operating Bandwidth	Center frequency (GHz)	Polarization	Number of element
[3]	17.0	-10 dB	6.4%	1.26	Single linear pol	8
[4]	N.A.	-10 dB	10.1%	9.9	Single linear pol	16
[23]	N.A.	N.A.	N.A.	1.413	Single linear pol	6
[24]	N.A.	-10 dB	1.1/4.4%	14/35	Single linear pol	4
[25]	11	-10 dB	10.5%	2.09	Circular pol	4
[26]	9	-10 dB	3.3%	3	Single linear pol	4
[27]	10.2	-10 dB	0.4%	5.5	Circular pol	4
Ours	14.4	-6 dB	16.0%	1.25	Dual linear pol	16

is applied to improve the operational frequency bandwidth. With the aid of the differential feed, the high isolation between the two polarizations has been achieved. Two Marchand baluns are properly arranged under the patch to excite the two pairs of differential feeds without increasing the antenna size. The customized hinge and the FPCB bridge make the antenna array deployable. One deployable array prototype is fabricated and tested. The operating band is from 1.15 GHz to 1.35 GHz. The isolation between the two polarization is over 30 dB. The peak gain of the two polarization are 14.4 dBi and 14.1 dBi respectively. Its deployment concept is presented. The size of the folded array is only 20% of the deployed one. Improvement can be made in the next version for higher mechanical reliability.

REFERENCES

[1] C. A. Balanis, *Antenna Theory: Analysis and Design*. Hoboken, NJ, USA: Wiley, 2016, pp. 598–614.
[2] J. Huang, "Paper-thin membrane aperture-coupled L-band antennas," *IEEE Trans. Antennas Propag.*, vol. 53, no. 8, pp. 2499–2502, Aug. 2005.
[3] A. Moussessian et al., "An active membrane phased array radar," in *IEEE MTT-S Int. Microw. Symp. Dig.*, Long Beach, CA, USA, Jun. 2005, pp. 1711–1714.
[4] M. R. M. Hashemi et al., "A flexible phased array system with low areal mass density," *Nat. Electron.*, vol. 2, no. 5, pp. 195–205, 2019.

[5] K. Ghorbani and R. B. Waterhouse, "Dual polarized wide-band aperture stacked patch antennas," *IEEE Trans. Antennas Propag.*, vol. 52, no. 8, pp. 2171–2175, Aug. 2004.
[6] A. Vallecchi and G. B. Gentili, "An inflatable deployable polarization agile microstrip antenna for space-borne synthetic aperture radar systems," in *Proc. IEEE Int. Symp. Phased Array Syst. Technol.*, Boston, MA, USA, Oct. 2003, pp. 76–81.
[7] F. Zhang, G.-M. Yang, Y.-Q. Jin, F. Peng, and J. Mo, "Space-borne deployable P-band dual-circular-polarization flexible antenna array," *IEEE Antennas Wireless Propag. Lett.*, vol. 16, pp. 2529–2533, 2017.
[8] G.-J. Xie, F.-S. Zhang, S.-B. Liu, and Y. Zhao, "A wideband dual-polarized aperture-coupled antenna embedded in a small metal cavity," *IEEE Trans. Antennas Propag.*, vol. 68, no. 11, pp. 7646–7651, Nov. 2020.
[9] K.-L. Wong and T.-W. Chiou, "Design of dual polarized patch antennas fed by hybrid feeds," in *Proc. 5th Int. Symp. Antennas Propag. EM Theory*, Beijing, China, Aug. 2000, pp. 22–25.
[10] T.-W. Chiou and K.-L. Wong, "Broad-band dual-polarized single microstrip patch antenna with high isolation and low cross polarization," *IEEE Trans. Antennas Propag.*, vol. 50, no. 3, pp. 399–401, Mar. 2002.
[11] K.-L. Wong and T.-W. Chiou, "Broadband dual-polarized patch antennas fed by capacitively coupled feed and slot-coupled feed," *IEEE Trans. Antennas Propag.*, vol. 50, no. 3, pp. 346–351, Mar. 2002.
[12] C.-Y.-D. Sim, C.-C. Chang, and J.-S. Row, "Dual-feed dual-polarized patch antenna with low cross polarization and high isolation," *IEEE Trans. Antennas Propag.*, vol. 57, no. 10, pp. 3405–3409, Oct. 2009.
[13] H. Saeidi-Manesh and G. Zhang, "High-isolation, low cross-polarization, dual-polarization, hybrid feed microstrip patch array antenna for MPAR application," *IEEE Trans. Antennas Propag.*, vol. 66, no. 5, pp. 2326–2332, May 2018.
[14] Q. Yang et al., "Millimeter-wave dual-polarized differentially fed 2-D multibeam patch antenna array," *IEEE Trans. Antennas Propag.*, vol. 68, no. 10, pp. 7007–7016, Oct. 2020.
[15] Y.-X. Guo, K.-W. Khoo, and L. C. Ong, "Wideband dual-polarized patch antenna with broadband baluns," *IEEE Trans. Antennas Propag.*, vol. 55, no. 1, pp. 78–83, Jan. 2007.
[16] H. Nawaz and I. Tekin, "Double-differential-fed, dual-polarized patch antenna with 90 dB interport RF isolation for a 2.4 GHz in-band full-duplex transceiver," *IEEE Antennas Wireless Propag. Lett.*, vol. 17, pp. 287–290, 2018.
[17] J. Lu, P. K. Tan, A. Liu, S. Sow, and T. H. Gan, "Collapsible, wide-band, dual-polarization patch antenna," in *Proc. IEEE Symp. Antennas Propag.*, Singapore, Dec. 2021, pp. 1219–1220.
[18] N. Marchand, "Transmission line conversion transformers," *Electronics*, vol. 17, no. 12, pp. 142–145, Dec. 1944.
[19] Z.-Y. Zhang, Y.-X. Guo, L. C. Ong, and M. Y. W. Chia, "A new planar Marchand balun," in *IEEE MTT-S Int. Microw. Symp. Dig.*, 2005, pp. 1971–1974.
[20] C.-H. Tseng and Y.-C. Hsiao, "A new broadband Marchand balun using slot-coupled microstrip lines," *IEEE Microw. Wireless Compon. Lett.*, vol. 20, no. 3, pp. 157–159, Mar. 2010.
[21] J. Lu, K.-S. Ang, and T.-H. Chio, "Low profile tapered slot array antenna," in *Proc. IEEE Int. Symp. Antennas Propag. Soc.*, Toronto, ON, Canada, Jul. 2010, pp. 1–4.
[22] W. Wang and Y. Zheng, "Wideband gain enhancement of high-isolation Fabry–Pérot antenna array with tandem circular parasitic patches and radial gradient PRS," *IEEE Trans. Antennas Propag.*, vol. 69, no. 11, pp. 7959–7964, Nov. 2021.
[23] C. G. Christodoulou, P. F. Wahid, M. R. Mahbub, and M. C. Bailey, "Design of a minimum-loss series-fed foldable microstrip," *IEEE Trans. Antennas Propag.*, vol. 48, no. 8, pp. 1264–1267, Aug. 2000.
[24] D. E. Anagnostou et al., "Development of a dual-frequency, dual-polarization, flexible and deployable antenna array for weather applications," presented at the IST Mobile Wireless Commun. Summit, Myconos, Greece, Jun. 2006.
[25] Z. Zhong, L. Xu, H. Zhang, and P. Zhang, "A foldable circular polarized microstrip antenna array for satellite communication," in *Proc. 12th Int. Symp. Antennas Propag. EM Theory*, Hangzhou, China, Dec. 2018, pp. 1–4.
[26] S. R. Seiler et al., "An origami inspired circularly-polarized folding patch antenna array," in *Proc. IEEE Int. Symp. Antennas Propag.*, Boston, MA, USA, Jul. 2018, pp. 181–182.
[27] P. Bouça, J. N. Matos, S. R. Cunha, and N. B. Carvalho, "Low-profile aperture-coupled patch antenna array for CubeSat applications," *IEEE Access*, vol. 8, pp. 20473–20479, 2020.